International Journal of Precision Engineering and Manufacturing-Green Technology (2019) 6:315–327
https://doi.org/10.1007/s40684-019-00060-1

Online ISSN 2198-0810
Print ISSN 2288-6206

REGULAR PAPER

Effect of Pulsed Electric Current on TRIP-Aided Steel

Hye-Jin Jeong[1] · Ju-won Park[1] · Kyeong Jae Jeong[1] · Nong Moon Hwang[1] · Sung-Tae Hong[2] · Heung Nam Han[1]

Received: 5 March 2018 / Revised: 29 June 2018 / Accepted: 18 July 2018 / Published online: 25 February 2019

Abstract

In the present study, the tensile deformation behavior of transformation-induced plasticity (TRIP)-aided steel under pulsed electric current is investigated. When a pulsed electric current is applied to the specimen during entire tensile deformation, a significant reduction of elongation is observed. The reason is that the mechanically induced martensitic transformation (MIMT) effect does not work properly as the stability of retained austenite phase increases due to temperature rise by the applied electric current. To improve the ductility of the TRIP-aided steel, the pulsing pattern of electric current is modified to apply the electric current only in the early stage of deformation immediately before the phase transformation of retained austenite phase begins to take place. As a result, the elongation is significantly increased by delaying the MIMT effect and making it work properly in the latter stage of deformation. Also, the electrically-induced annealing effect, which occurs in the early stage of deformation where a dislocation plasticity occurs dominantly, contributes to the improvement of elongation. The modified pulsing pattern suggested in the present study provides an easy-to-implement technique to improve the formability of the TRIP-aided steel.

Keywords TRIP-aided steel · Formability · Electroplastic effect · Electrically assisted Manufacturing (EAM) · Mechanically induced martensitic transformation (MIMT)

1 Introduction

Recently, demands for weight reduction in many automotive industries have been driving the development of advanced high-strength steels (AHSSs) with high strength-to-weight ratios. This is due not only to improvements in fuel efficiency, but also to the consumer's increasing demand for safer and more comfortable vehicle [1, 2]. To satisfy these demands, steel makers are trying to increase the strength of steels without significantly deteriorating their ductility by generating multiphase microstructures [3, 4]. One of the various AHSSs containing multiphase is transformation-induced plasticity (TRIP)-aided steel, which consists of a ferrite, metastable retained austenite, bainite and martensite phases [5, 6]. Note that TRIP refers to a phenomenon in which a permanent strain remains after the solid–solid phase transformation under external stress [7, 8]. The retained austenite phase in the TRIP-aided steel transforms into hard martensite phase, which is induced mechanically by an external stress or strain, leading to higher ductility due to a delay effect of necking (TRIP effect) [9]. This phase transformation proceeding by an external stress or strain is hereafter denoted as the mechanically induced martensitic transformation (MIMT). Thus, TRIP-aided steels containing a large volume fraction of retained austenite phase are preferred types of AHSSs [10].

However, TRIP-aided steel with a high strength still shows large springback and forming load during forming,

✉ Heung Nam Han
hnhan@snu.ac.kr

Hye-Jin Jeong
hj8262@snu.ac.kr

Ju-won Park
pjw1842@snu.ac.kr

Kyeong Jae Jeong
jkj4512@snu.ac.kr

Nong Moon Hwang
nmhwang@snu.ac.kr

Sung-Tae Hong
sthong@ulsan.ac.kr

[1] Department of Materials Science and Engineering and RIAM, Seoul National University, 1, Gwanak-ro, Gwanak-gu, Seoul 08826, South Korea

[2] School of Mechanical Engineering, University of Ulsan, 93, Daehak-ro, Nam-gu, Ulsan 44610, South Korea

which make it difficult for automakers to manufacture automotive parts in desired shapes with a reasonable cost. Furthermore, for TRIP-aided steel, it is well established that the MIMT effect takes place between the M_s (martensite start temperature) and the M_d (stress-induced martensite start temperature), above which the austenite becomes completely stable [11–13]. Therefore, there is a temperature between M_s and M_d, at which the MIMT effect is suppressed moderately and the resultant strain hardenability is held in a large strain range, leading to maximum benefit of the MIMT effect. However, in terms of warm and hot forming process, the process temperature, which is generally between 550 and 850 °C, is higher than M_d (200–400 °C) [14]. Thus, the MIMT effect could not work properly in the hot forming process of the TRIP-aided steels. Additionally, the hot forming process inevitably induces increased adhesion between the material and the die, decreased die strength, surface oxidation, and low production efficiency.

To overcome these problems, the electrically assisted manufacturing (EAM) technique can be suggested as a promising new forming method for TRIP-aided steels. The EAM technique may alter the microstructure and improve the mechanical property of metal alloys by applying high electric current to the materials during deformation. Note that the effect of the electric current on the metals during deformation is often called the electroplastic effect. Many researchers have carried out researches to understand the electroplastic effect on mechanical behavior and microstructure. The influence of the electroplastic effect was first reported by Troistkii [15] in 1969. Conrad et al. [16, 17] conducted a series of extensive studies on the electroplastic effect in various metals, supporting the fact that high electric current can clearly enhance the ductility of metals in addition to the side effect of Joule heating. Ross and Roth [18, 19] also investigated the effect of electric current on various metal alloys including aluminum alloy, copper alloy, and brass alloy. Recently, Kim et al. [20] observed the acceleration of dislocation annihilation by applying pulsed electric current during tensile tests of 5052 aluminum alloy, resulting in a large increase in the elongation.

Furthermore, there have been many cases of applying electric current to high-strength steels [21–25]. Tang et al. [21] reported that the drawing stress of stainless steel wire was decreased by approximately 20–50% with the application of electric current pulses, showing the improvement in plasticity. Kim et al. [22] studied the effect of electric current density on the mechanical properties of AHSS under quasi-static tensile loads. The authors reported that the electric current can be effectively used to reduce the springback of the material. Lu and Qin [23] also investigated the effect of electric current on the tempering of martensite in dual-phase steels. The authors indicated that high electric current can significantly enhance the strength of tempered dual-phase steels via the formation of ultrafine-grained ferrite with nanocementite particles.

The fundamental mechanism about these electroplastic effects has not been identified yet. Several electroplasticity hypothesis have been proposed to explain the mechanical behavior during electrically assisted deformation. One of them, the mechanical behavior of metals under an electric current could be described satisfactorily in terms of the thermal effects of Joule heating [26, 27]. However, it also has been reported that the electroplasticity cannot be clearly understood without any consideration of the athermal effect, which is distinct from the Joule heating, such as electric current-induced annealing [20], aging [28] dissolution [29], and recrystallization [30]. They share one common idea that the electric current can enhance mobility of metal atoms resulting in accelerating the diffusion kinetics [20, 28–33].

Based on the positive effects of electric current on the plastic deformation, Liu et al. [34] applied the electric current to TRIP-aided steel during tensile test. However, the authors observed that the ductility was not improved by applying electric current, despite of the reduction in flow stress. This was explained by the suppression of the MIMT effect due to the increased temperature [34]. Unfortunately, the technique, which can improve the formability of TRIP-aided steel by applying electric current, has not been developed until now. In the present study, the effect of electric current on the MIMT during tensile deformation is investigated and a modified pulsing pattern of electric current is suggested based on the microstructural observation to improve the formability of TRIP-aided steel.

2 Experimental Set-up

The chemical composition of the investigated TRIP-aided steel is Fe-0.35C-3.68Mn-0.19Si-5.27Al in wt.%. The higher Al content in this alloy than other conventional TRIP-aided steels provides a density reduction effect by means of substitution and lattice expansion. Typical tensile specimens (ASTM-E08) with a gauge width of 6.25 mm, thickness of 1 mm, and gauge length of 25 mm were fabricated along the rolling direction of the sheet.

Quasi-static uniaxial tensile tests were conducted using the experimental set-up described in Fig. 1a with a constant crosshead speed of 1.5 mm/min (corresponding to the nominal strain rate of 1×10^{-3}/s) at room temperature (RT 25 °C). The tensile test machine (INSTRON 5584, USA) was modified to apply electric current only through the specimen by inserting Bakelite (Insulator) between the specimen and each grip. The displacement of the specimen was measured by ARAMIS Digital Image Correlation (DIC) system (GOM, Germany), which provides non-contact measurement based on the principle of digital image correlation. Note that the

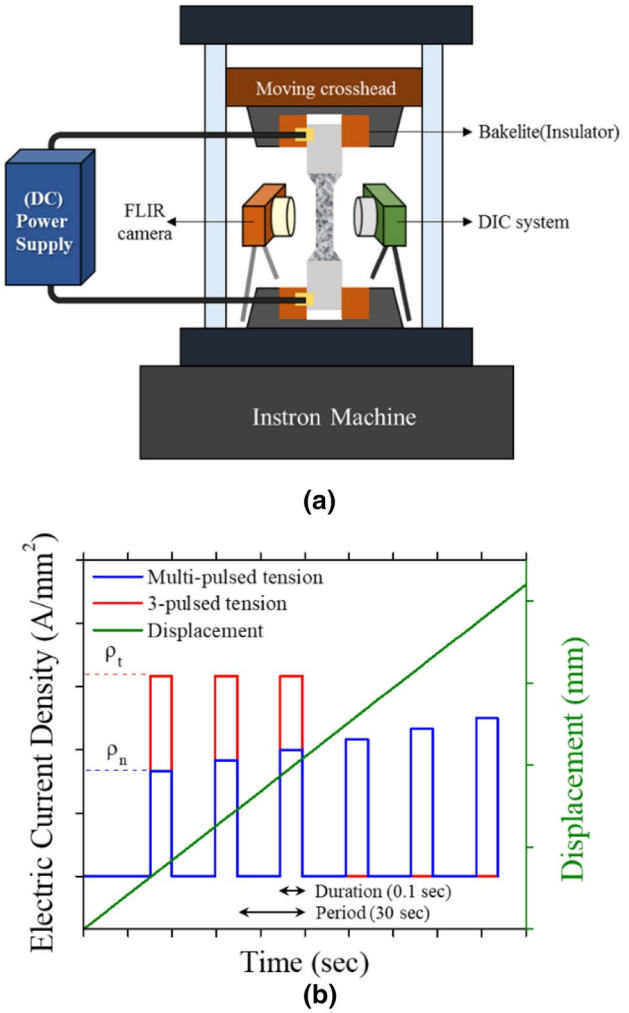

Fig. 1 Schematics of **a** experimental set-up for non-pulsed/pulsed tensile tests and **b** two types pulsing conditions applied to the specimen during uniaxial tensile test

experimental set-up described in Fig. 1a is identical to that described in the previous studies [20, 28, 29].

The pulsed tensile tests were carried out by using two pulsing patterns of electric current, and the electric current was generated by a Vadal SP-1000U welder (Hyosung, South Korea). First, the electric current was periodically applied to the specimen with a duration (t_d) of 0.1 s and a period (t_p) of 30 s during deformation (multi-pulsed tension), as schematically shown in Fig. 1b. The first pulse of electric current was applied immediately before yielding. The amplitude of the electric current was selected to induce a nominal electric current density (ρ_n) of 50 A/mm^2 based on the original cross-sectional area of the specimen. Note that as the specimen is continuously deformed by tension, the cross sectional area of the gage continuously decreases. Therefore, with the constant amplitude of electric current, the true electric current density (ρ_t) based on the actual cross-sectional area for each pulse of electric current continuously increases. Second, the tensile test with three pulses of electric current (3-pulsed tension) was conducted under the condition of a duration (t_d) of 0.1 s and a true electric current density (ρ_t) of 95 A/mm^2, as schematically shown in Fig. 1b. The first pulse of electric current was applied immediately before yielding. Three pulses of electric current were applied to the specimen only in the early stage of deformation, when the phase transformation of retained austenite phase begins to take place. In order to maintain a constant electric current density (ρ_t) based on the initial cross-sectional area of the specimen, a different amplitude of electric current was applied to the specimen considering the decrease in cross-sectional area of the specimen during deformation.

The non-pulsed tensions at high temperature were also performed using the same tensile machine with an environmental chamber at cross-head speed 1.5 mm/min. Target temperatures was set to 100 and 200 °C, which cover the temperature range measured during the multi-pulsed and 3-pulsed tension, to evaluate the thermal effect due to Joule heating on the mechanical behavior. Test was performed after the target temperature was reached.

The temperature change of the specimen during the pulsed tensile test was measured using an FLIR-E40 infra-red (IR) thermal imaging camera (FLIR, Sweden). One side of the specimen was sprayed with black thermal paint to stabilize the emissivity and thus to improve the accuracy of temperature measurement. The emissivity was calibrated by comparing the measured temperature using a K-type thermocouple. The temperature was measured for the middle part of the specimen, which is the highest-temperature part when the electric current was applied to the specimen.

The microstructure of the initial specimen was characterized by a JXA- 8530F electron probe microanalyzer (EPMA, JEOL Ltd., Japan) and a field emission gun scanning electron microscope (FE-SEM, SU70, Hitachi, Japan) equipped with an electron backscatter diffraction (EBSD) system (EDAX/TSL, Hikari, USA). To calculate the M_s temperature, the quantities of carbon (C), aluminum (Al), silicon (Si), and manganese (Mn) in the retained austenite phase were obtained from the EPMA analysis. The X-ray diffraction (XRD) measurement was carried out using a Lab X-ray diffractometer (Smart Lab, Rigaku, Japan) with a Mo radiation source operating at 50 kV at RT. The diffraction patterns were recorded in the angular range of 18°–36° with a scan rate of 1°/min. The phase identification was performed by matching the peak positions and relative intensities with PDF reference data. To check the change in dislocation density during the pulsed tensile test, the full width at half maximum (FWHM) value was obtained from the X-ray diffraction peak data. The diffraction peaks could be fitted well

with the Pseudo-Voigt function. In order to measure the fraction of the retained austenite phase, a Rietveld refinement was performed for all specimens using the TOPAS (version 4.2) software package. The specimens for microstructure observation were prepared by mechanical grinding followed by electropolishing with a 100 ml perchloric acid and 900 ml ethanol solution. For the EBSD analysis, the accelerating voltage and scan step size were 15 kV and 0.4 μm, respectively. The critical misorientation angle was set to 15° for grain identification.

3 Results and Discussion

3.1 Initial Properties

Figure 2a, b show the EBSD inverse pole figure (IPF) and phase maps for the investigated TRIP-aided steel. The different colors in the IPF map indicate the orientation of each grain with respect to normal direction (ND). The initial specimen consists of a ferrite matrix (green area) with some retained austenite grains (red area). The average grain sizes of the ferrite and retained austenite phase were 7.2 and 2.0 μm, respectively. The volume fraction of these retained austenite phase is 24.5%, which was measured from EBSD analysis. In order to ensure the reliability and accuracy of the data, an additional XRD measurement was conducted. The X-ray diffraction pattern of the initial specimen was presented in Fig. 2b. The (111), (200), and (220) peaks of the austenite phase were identified under the given measurement condition. The (110), (200), and (210) peaks of the ferrite phase were also identified. Through the Rietveld method using TOPAS, the volume fraction of austenite phase was determined to be approximately 26.5%. The discrepancy of the phase fraction might originate from the limitation of the EBSD analysis, which is performed only on the surface of the specimen. Thus, the value obtained from XRD measurement (26.5%) was used as reference value in this study.

Figure 3 shows the backscattered electron micrograph and distributions of C, Al, Si, and Mn in the initial specimen which were obtained from the EPMA analysis. As a result, the measured concentrations of C, Mn, Al, and Si in the retained austenite phase were 1.21, 5.76, 4.18, and 0.06 wt.%, respectively. The concentrations of C and Mn in the

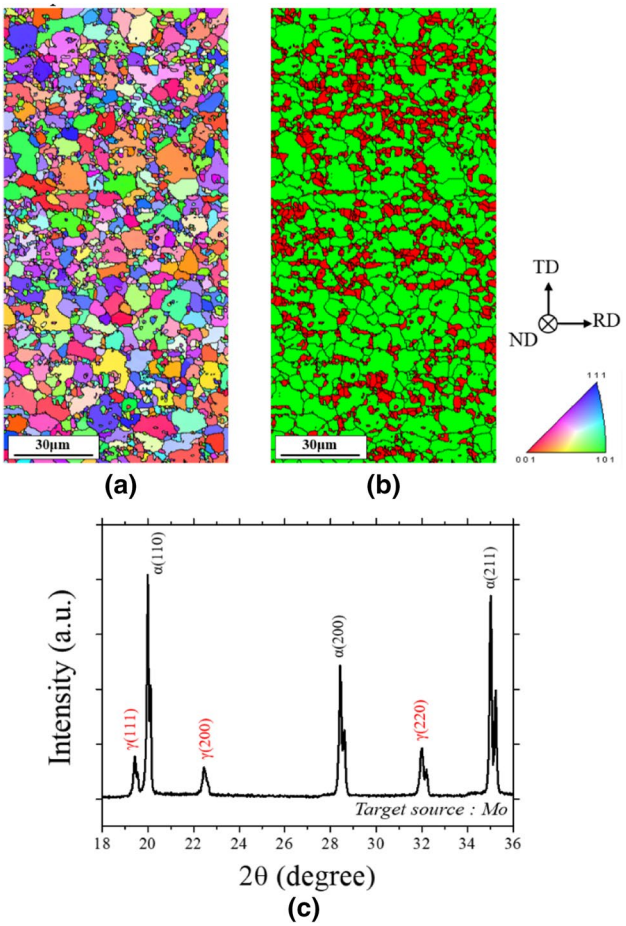

Fig. 2 **a** EBSD inverse pole figure map for normal direction (ND), **b** EBSD phase map (red area: retained austenite phase, green area: ferrite matrix), and **c** X-ray diffraction pattern in the range of 18-36° for the investigated TRIP-aided steel

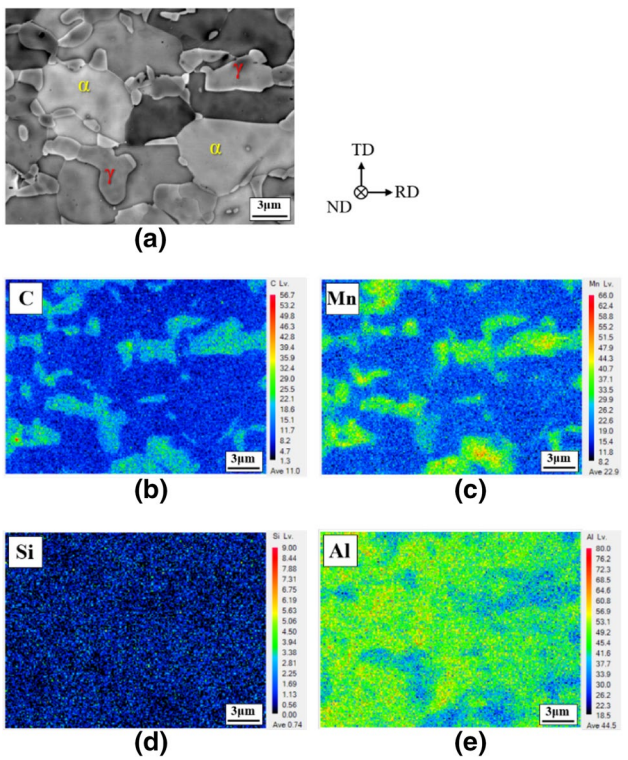

Fig. 3 Elements distribution in the initial specimen: **a** backscattered electron image, **b** C distribution, **c** Al distribution, **d** Si distribution, and **e** Mn distribution

retained austenite phase were much higher than the nominal concentration (0.35 and 3.68 wt.%, respectively), as shown in Fig. 3b, c. This showed good agreement with the fact that C and Mn concentrate in the retained austenite phase accompanying the ferrite and bainite phase transformation for TRIP-aided steels [35]. On the contrary, it was observed that Al and Si were slightly concentrated on the ferrite phase compared with the retained austenite, as shown in Fig. 3d, e.

Based on the concentration of elements in the retained austenite phase determined quantitatively from the EPMA analysis, the M_s temperature of the retained austenite in this material was calculated to be − 22 °C using the following equation [36]:

$$M_s(^{\circ}\mathrm{C}) = 539 - 423C - 30.4Mn - 7.5Si + 30Al, \quad (1)$$

where C, Mn, Si, and Al are the contents of these elements in wt.%. It is clear that the M_s temperature is lower than the RT (25 °C). Thus, the austenite phase in the investigated TRIP-aided steel can remain metastable at RT.

3.2 Mechanical Behavior with Periodic Pulsed Electric Current

In the non-pulsed tension, the specimen showed strain hardening after yielding at ~ 500 MPa and failed by fracture at the true strain of 0.33, as shown in Fig. 4a. In the multi-pulsed tension, the flow stress decreased rapidly immediately after each pulse and then increased owing to strain hardening until the next pulse, as shown in Fig. 4a. The decrease in flow stress by applied electric current is known to be caused by thermal and athermal effects, as described in Jeong et al. [33]. When compared to the non-pulsed specimen, the multi-pulsed specimen showed a reduction in ductility in spite of the decrease in flow stress. The elongation decreased from 0.33 to 0.26. Under the non-pulsed tension at 100 °C, the flow stress decreased and the elongation also decreased from 0.33 to 0.25, compared with the non-pulsed tension at RT. There is no significant difference between the multi-pulsed tension and non-pulsed tension at 100 °C with respect to the flow stress and elongation at fracture.

The measured specimen temperature during the multi-pulsed tension is presented in the Fig. 4b. During an electric pulse application, the specimen temperature increased instantly due to the Joule heating effect. After applying the electric pulse, the specimen temperature decreased by air cooling until the next pulse. The peak value of the measured temperature showed a steady increase owing to the continuously increasing true electric current density with decreasing cross-sectional area during deformation.

For the multi-pulsed tension and non-pulsed tension at 100 °C, it was observed that the slope of true stress-strain curve noticeably changed in comparison with the non-pulsed tension at RT. The slope of the stress-strain curve indicates

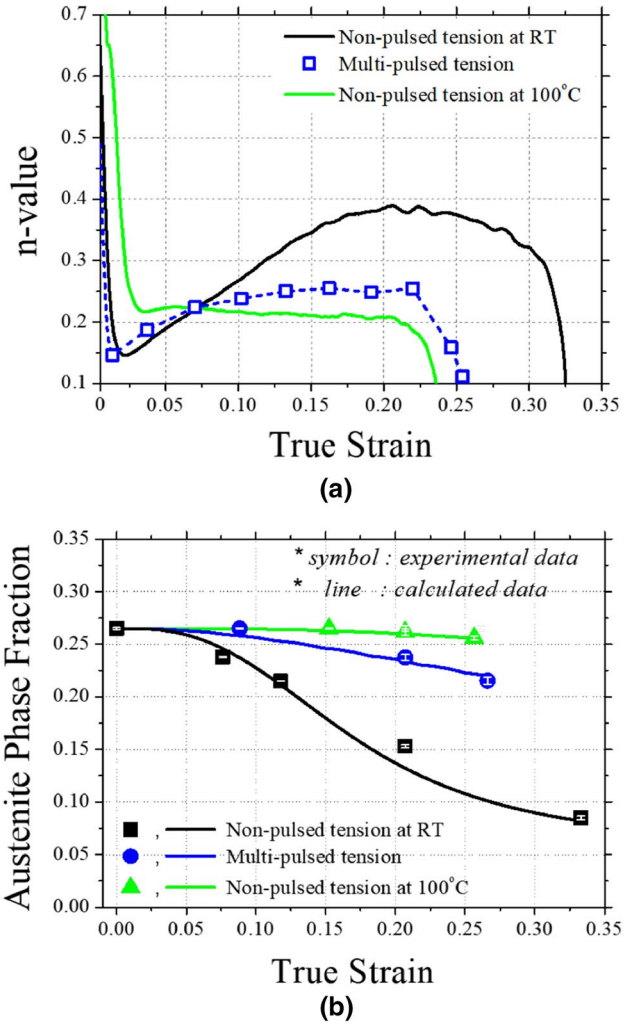

Fig. 4 **a** The calculated strain hardening exponent and **b** the fraction of retained austenite phase as a function of true strain for non-pulsed tension at RT (in black), non-pulsed tension at 100°C (in green), and multi-pulsed tension (in blue). The experimental data (symbols) and calculated data (lines) were based on the XRD measurement and MIMT kinetics model, respectively

the strain hardening rate, which is called the strain hardening exponent (n). The strain hardening exponent can be expressed as true stress (σ) and true strain (ε):

$$n = \frac{d\ln\sigma}{d\ln\varepsilon}. \quad (2)$$

The change in hardening rate of TRIP-aided steels is related to the volume fraction of mechanically induced martensite phase [10, 12]. The increase in the fraction of the hard martensite phase with increasing true strain induces the increase in the hardening rate. This increase in the hardening rate due to the fraction of hard martensite phase is denoted as phase hardening, according to Han et al. [12].

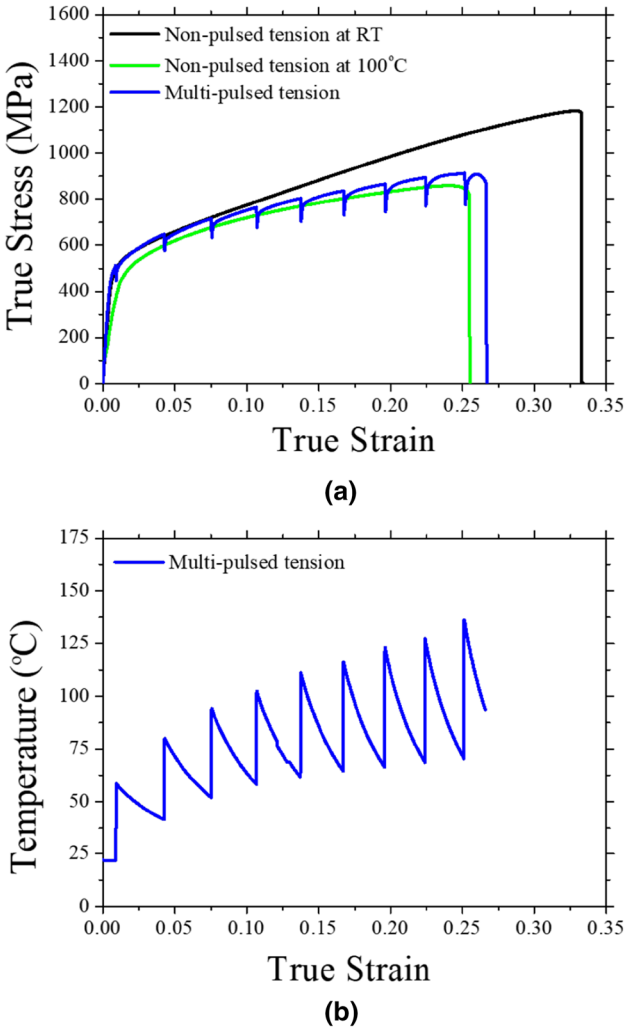

Fig. 5 **a** True stress-strain curves of non-pulsed tension at RT (in black), non-pulsed tension at 100°C (in green), and multi-pulsed tension (in blue) under the cross head speed of 1.5 mm/min. **b** The temperature of specimen measured during multi-pulsed

To check the influence of electric current on the phase hardening effect, the strain hardening exponent was calculated and plotted as a function of true strain in Fig. 5a. In the non-pulsed tension at RT, the strain hardening exponent increased until the true strain was approximately 0.2, and the maximum value was approximately 0.4. However, in the non-pulsed tension at 100 °C, the value of strain hardening exponent gradually decreased as the deformation progressed. For the multi-pulsed tension, it is difficult to compare the strain hardening exponent properly due to the stress drop phenomenon caused by applying periodic electric current. Thus, considering only the maximum flow stress points in the strain hardening zones where the electric current was eliminated, the strain hardening exponent values were calculated and are shown as symbols in Fig. 5a. The line connecting the symbols is presented by the dotted line in Fig. 5a. It was identified that the strain hardening exponent value under the multi-pulsed tension was significantly lower than that under the non-pulsed tension at RT, although it showed a slight increase as the deformation progressed. This suggests that the phase hardening effect did not occur, owing to the suppression of the MIMT effect caused by a temperature increase under the given condition of multi-pulsed tension.

To quantitatively investigate the suppression effect of the MIMT by applying electric current, the microstructural changes were analyzed as the deformation progressed, focusing on the change in the retained austenite phase fraction. As shown in Fig. 5b, for the non-pulsed tension at RT, the fraction of the retained austenite phase decreased as the deformation progressed. The fractions of the retained austenite phase at the true strains of 0.076, 0.117, and 0.207 were 23.8, 21.5, and 15.3%, respectively. For the specimen immediately after fracture, the retained austenite phase fraction of 8.5% remained. This means that the retained austenite phase obviously transformed into martensite phase during deformation at RT. However, in the multi-pulsed tension, the retained austenite phase fraction slightly decreased as the deformation progressed. The fraction of the retained austenite phase in the multi-pulsed specimen immediately after fracture was 21.5%, which was much higher than that in the non-pulsed tension at RT (8.5%). For the non-pulsed tension at 100 °C, there is no noticeable change in the fraction of the retained austenite phase during the deformation. This indicates that the MIMT effect hardly worked, because the stability of the retained austenite phase increased due to the temperature rise under the conditions of multi-pulsed and non-pulsed tension at 100 °C.

Based on these results, it can be seen that periodically applying multi pulses of electric current to the specimens interferes with the MIMT effect and causes the ductility to decrease, as shown in Fig. 4a. Therefore, a new design of electric current pulsing pattern should be developed for improving the formability of TRIP-aided steel without requiring additional processing.

3.3 Mechanical Behavior with Three Pulses of Electric Current in the Early Stage of Deformation

For improving the ductility of the TRIP-aided steel, the pulsing pattern of electric current was modified to apply three pulses of electric current in the early stage of deformation immediately before the phase transformation of retained austenite phase begins. The point at which to apply electric current was selected to be before an inflection point. Note that the MIMT occurred significantly at the inflection point according to the result in Fig. 5b. Thus, based on the inflection point occurring at a true strain of approximately 0.10, the three pulses of electric current were applied at the

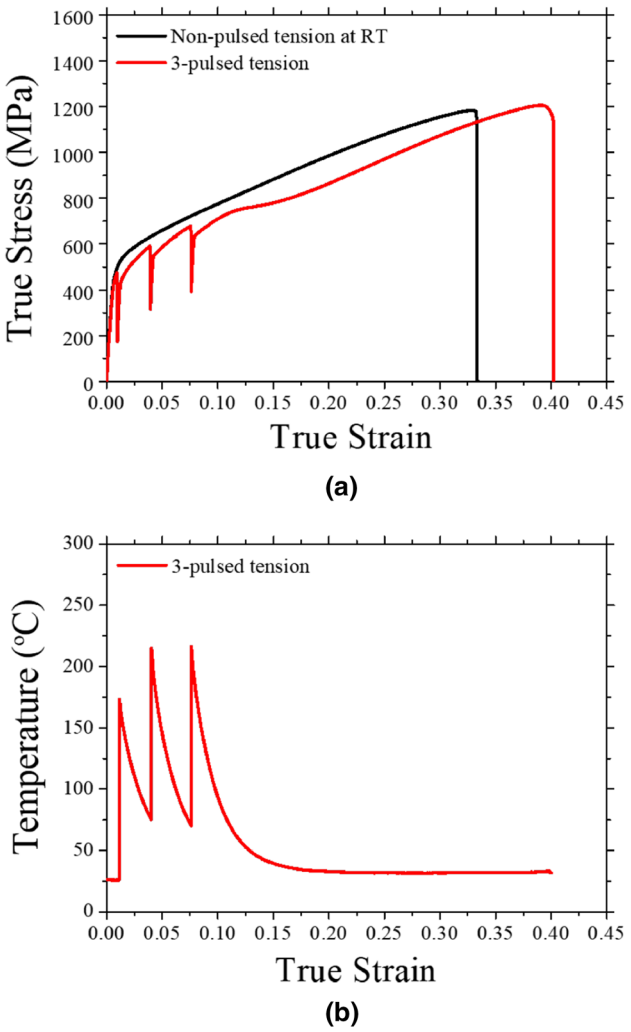

Fig. 6 **a** True stress-strain curves of non-pulsed tension at RT (in black) and 3-pulsed tension (in red) under the cross head speed of 1.5 mm/min. **b** The temperature of specimen measured during 3-pulsed tensile test

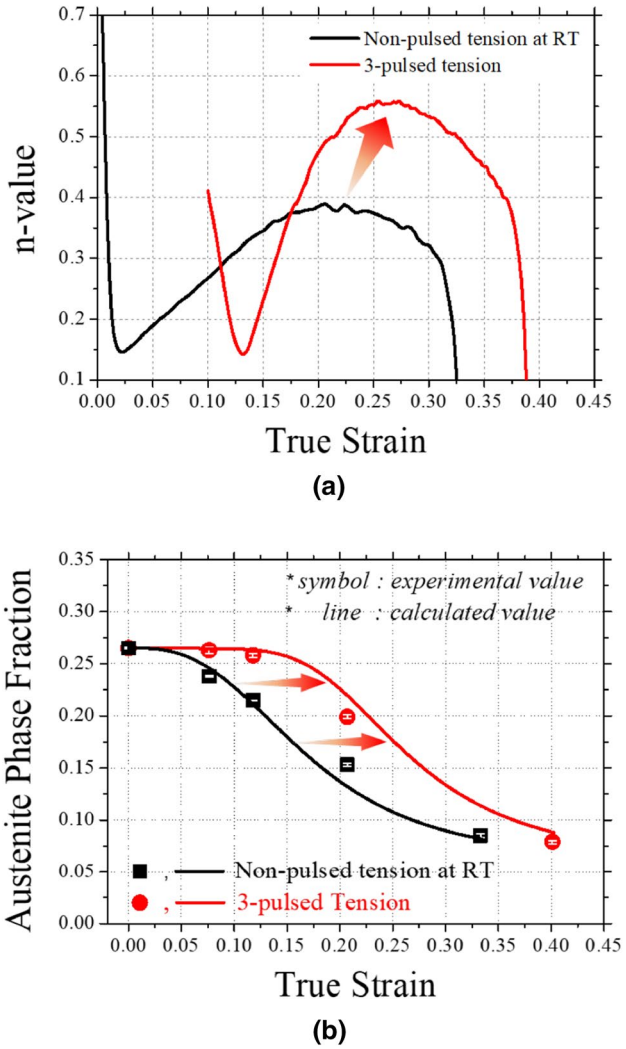

Fig. 7 **a** The calculated strain hardening exponent and **b** the fraction of retained austenite phase as a function of true strain for the non-pulsed tension at RT (in black) and 3-pulsed tension (in red). The experimental data (symbols) and calculated data (lines) was based on the XRD measurement and MIMT kinetics model, respectively

true strains of 0.01, 0.039, and 0.076, respectively. Moreover, in order to maintain the same electrical energy per unit volume, the electric currents were applied to the specimen while maintaining constant current density. As a result, the 3-pulsed specimen showed a significant increase in elongation, as shown in Fig. 6a. The elongation increased from 0.33 to 0.40 by applying only three pulses of electric current compared to the non-pulsed tension at RT. The flow stress in the 3-pulsed tension was much lower than that in the non-pulsed tension at RT. Figure 6b shows the measured specimen temperature during the 3-pulsed tension. The peak values of the measured temperature at each electric pulse were 170, 215, and 216 °C, respectively. Because the true current density was maintained as constant, the measured specimen temperature should theoretically be the same. However, since the first pulse was applied at RT and the second pulse was then applied at the state in which the specimen had not completely cooled to RT, it is thought that a difference in the measured temperature occurred.

In the 3-pulsed tension, it was also observed that the slope of the true stress-strain curve after applying three pulses was noticeably changed in comparison with the non-pulsed tension at RT. To check the effect of three pulses on the phase hardening effect, the strain hardening exponent (n) was calculated and is plotted as a function of true strain in Fig. 7a. The calculation was performed from the true strain of 0.10 after applying three pulses due to a large fluctuation by stress drop. As a result, in the 3-pulsed tension, the curve of strain hardening exponent was significantly different from

the non-pulsed tension at RT. The n value decreased to 0.13 until the true strain was 0.13, and then increased to 0.56 until the true strain was 0.26. When the three pulses were applied in the early stage of deformation, the maximum value of n appeared in the latter stage of deformation and increased in comparison with the non-pulsed tension at RT. This means that because the phase transformation from the retained austenite to the martensite phase was delayed by applying electric current, the phase hardening effect was amplified in the latter stage of deformation. This delay effect of phase transformation was caused by the increase in stability of the retained austenite phase during electric current application, as mentioned in Sect. 3.2.

To clarify the phase transformation delay effect by applying three pulses of electric current, the change in retained austenite phase fraction was measured based on the XRD measurement, as shown in Fig. 7b. In the 3-pulsed tension, it was observed that the curve of retained austenite phase fraction as a function of true strain was shifted to the right compared to the non-pulsed tension at RT. The fraction values of retained austenite phase for the 3-pulsed tension at the true strains of 0.076, 0.117, and 0.207 were 26.3, 25.8, and 19.8%, respectively. Since the fraction value of the retained austenite phase at the true strain of 0.117 was similar to the initial value (26.5%), it can be seen that the phase transformation hardly occurs up to the true strain of 0.117 under the application of electric current. From the true strain of 0.117, the fraction value of the retained austenite phase decreased in earnest, while the MIMT occurred properly. Moreover, at the true strain of 0.207, the fraction value of retained austenite phase in the 3-pulsed tension was still higher than that in the non-pulsed tension at RT. Thus, it was confirmed that applying the electric current in the early stage of deformation clearly induces the delay effect of MIMT.

In addition, for the specimen immediately after fracture in the 3-pulsed tension, the retained austenite phase fraction was 7.9%, which was similar with that in the non-pulsed tension at RT (8.5%). Moreover, there is no difference in the maximum true stress values at fracture between the non-pulsed tension at RT and 3-pulsed tension, as shown in Fig. 6a. This means that there is no negative effect of electric current on the implementation of the original mechanical properties for the investigated TRIP-aided steel.

3.4 Electric Current-Induced Annealing Effect

According to the study of Kim et al. [20], when a pulsed electric current was applied during deformation, the Al–Mg alloy was annealed due to the annihilation of dislocations. For the reasons of this annealing by applying electric current, two kinds of effect were suggested, which are thermal and athermal effects (electric current-induced annealing effect). In the present study of the TRIP-aided steel, under application of an electric current, the flow stress also decreased compared to the non-pulsed tension at RT, as shown in Figs. 4a and 6a. This implies a possibility that the annealing effect may occur by applying an electric current during deformation, as with the Al–Mg alloy. Therefore, the fact that annealing would take place under the given condition should be verified in this study.

The FWHM analysis of the diffraction peak profile is a well-established technique for determining the dislocation density in crystalline materials. Generally, diffraction peak profile is broadened when subgrains are small or if the crystal lattice is distorted by lattice defects, especially by dislocations [37–39]. Here, instrumental effects on the

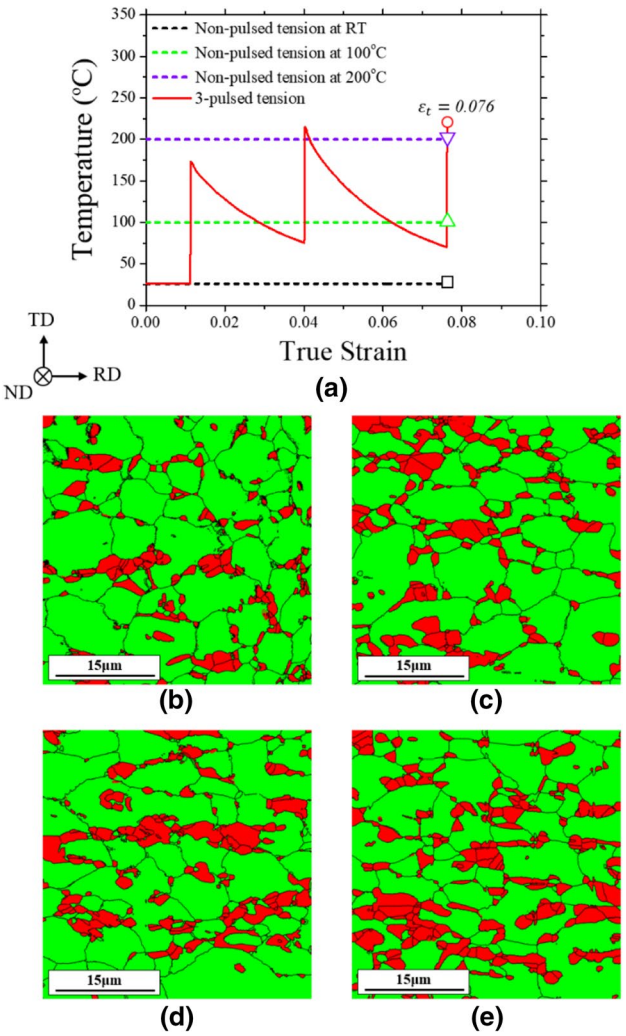

Fig. 8 **a** Temperature histories during 3-pulsed tension (in red), non-pulsed tension at RT (in black), 100°C (in green) and 200°C (in purple) until the true strain of 0.076. EBSD phase maps (red area: retained austenite phase, green area: ferrite matrix) for the four specimens obtained from: **b** the non-pulsed tension at RT, **c** the non-pulsed tension at 100°C, **d** the non-pulsed tension at 200°C, and **e** the 3-pulsed tension

diffraction peak broadening were assumed to be the same in all specimens, with a focus on the major effects of dislocations. Additionally, since the fraction of martensite phase and grain size can affect the FWHM value, the specimens containing the same fraction of martensite phase and grain size should be compared.

As shown in Fig. 8a, four specimens strained to the true strain of 0.076 in the non-pulsed tensions at RT, 100, 200 °C, and 3-pulsed tension were prepared to obtain the FWHM values of the ferrite peaks. From the XRD analysis results, it was identified that three specimens excluding the non-pulsed specimen at RT have the same fraction of retained austenite phase (26.5%), which means that there is no change in phase fraction until the true strain reached 0.076 under the three given conditions (non-pulsed tensions at 100, 200 °C, and 3-pulsed tension). Additionally, EBSD analysis was conducted for the four specimens to verify whether the grain size of the ferrite phase was same for the four specimens. Figure 8b–e show the phase map obtained from the non-pulsed tensions at RT, 100, 200 °C, and 3-pulsed tension, respectively. The ferrite and austenite phase are indicated by green and red, respectively. As a result, the average grain size of the ferrite phase for the four specimens obtained from the non-pulsed tensions at RT, 100, 200 °C, and 3-pulsed tension were almost the same as 6.44, 6.79, 6.13, and 6.28 μm, respectively (Fig. 8b–e).

Thus, the annealing effect was then qualitatively discussed by comparing of the FWHM values of the ferrite peaks for the four specimens under the same instrumental conditions, retained austenite phase fraction, and grain size.

The FWHM profiles obtained from the non-pulsed tensions at RT, 100, 200 °C and 3-pulsed tension at the same true strain of 0.076 are presented in the Fig. 9, as well as the X-ray diffraction patterns. The FWHM values are presented as a function of 2θ, where θ is the Bragg angle. As a result, for the non-pulsed tension, the values of FWHM decreased with increasing temperature. This was due to recovery effect of dislocation as the temperature increased. However, the values of FWHM obtained from the specimen in the 3-pulsed tension was lower than the non-pulsed tension at 100 °C and similar to the non-pulsed tension at 200 °C. Note that the strained specimen at 200 °C was deformed under stronger temperature condition, with respect to thermal energy, than the temperature condition of specimen due to Joule heating during 3-pulsed tension. This suggests that the specimen was clearly annealed due to the annihilation of dislocations by both thermal and athermal effects while three pulses of electric current were applied.

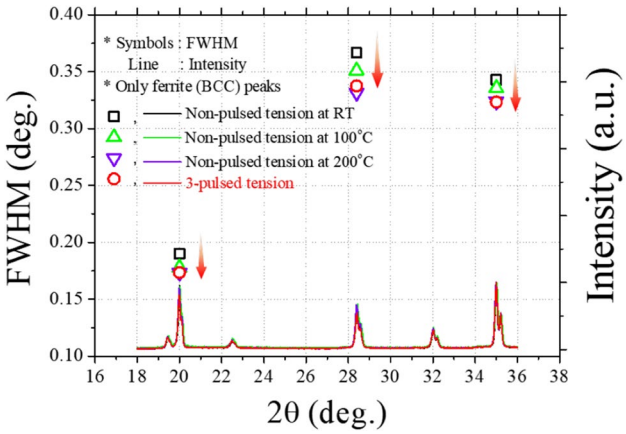

Fig. 9 FWHM profiles (symbols, left axis) of ferrite phase peaks and X-ray diffraction patterns (lines, right axis) in the range of 18°–36° for the four specimens strained to the true strain of 0.076 in the 3-pulsed tension (in red), non-pulsed tension at RT (in black), 100°C (in green) and 200°C (in purple)

Based on this result, it is thought that the electric current-induced annealing would also occur in the multi-pulsed tension. However, when multi pulses of electric current were applied, the suppression of the MIMT effect overwhelmed the electric current-induced annealing effect so that the ductility was decreased.

Therefore, applying an electric current at the state in which the phase transformation of the retained austenite phase begins to take place can clearly induce both the electric current-induced annealing and an adequate delay of the MIMT effects. This enhances the ductility without deteriorating of mechanical property. Thus, it was confirmed that the formability of TRIP-aided steel can be sufficiently improved by applying an electric current. Furthermore, our results show that the EAM technique can save a lot of energy and time in the forming of TRIP-aided steel.

3.5 Calculation for MIMT Kinetics

In addition to the experimental measurement of the retained austenite phase fraction, a calculation of the MIMT kinetics in both non-pulsed and pulsed tensions was performed using the model, which was derived based on the concept of energetically favorable variant selection under an external stress field [40]. In this model, the chemical free energy change, ΔG, and the entropy change, ΔS, were defined in terms of the thermodynamic theory for the austenite-to-martensite transformation. The mechanical interaction energy, U^i, for the ith martensitic variant between the externally applied stress and the lattice deformation in austenite during phase transformation can be defined as the product of applied stress and the transformation strain for the ith martensitic variant. Han et al. [40] derived the following expression for the increment of the extended martensite volume fraction in the retained austenite, df_{ex}^i :

$$df_{ex}^i = A^i d\bar{\varepsilon}_a^P + Bd(XH(-dX))H(-dX)H\left[\left(\Delta G^C - X\right)\right], \quad (3)$$

where X is $\Delta G + U^i$ and $d\bar{\varepsilon}_a^P$ is the effective plastic strain increment accumulated in the parent austenite. In the present study, the value of $d\bar{\varepsilon}_a^P$ was calculated reflecting strain partitioning effect during deformation based on the ratio of the hardness value for each phase in the TRIP-aided steel. Thus, the value of $d\bar{\varepsilon}_a^P$ was calculated using the following equation:

$$d\bar{\varepsilon}_{total}^P = d\bar{\varepsilon}_f^P + d\bar{\varepsilon}_a^P + d\bar{\varepsilon}_m^P, \tag{4}$$

where $d\bar{\varepsilon}_{total}^P$, $d\bar{\varepsilon}_f^P$, and $d\bar{\varepsilon}_m^P$ are the total plastic strain increment, the effective plastic strain increments accumulated in the ferrite and martensite phases, respectively. The $d\bar{\varepsilon}_{total}^P$ value was taken from the experimental data obtained from the true stress-strain curve. It was reported that the nano-hardness value of the martensite phase is four times higher than that of the ferrite phase [41]. Thus, the effective plastic strain during tensile deformation was assumed to be inversely proportional to the hardness of each phase. For the simplicity of calculation, it was also assumed that the hardness of the ferrite phase is the same as that of the austenite phase. In Eq. (3), H is the Heaviside step function, reflecting the fact that the martensitic transformation can occur when the driving force exceeds the critical free energy. ΔG should be defined as a function of temperature. ΔG^C is known to be 2100 J/mol regardless of chemical composition according to Jaccin and Beyer [42]. Under the assumption that ΔG is a linear function of temperature, ΔG and ΔS can be derived as follows:

$$\Delta G = \Delta G^C + \Delta S\left(T - M_s\right), \tag{5}$$

$$\Delta S = -\Delta G^C/(T_0 - M_s), \tag{6}$$

where T_0 is the temperature at which the difference in the chemical free energy between austenite and martensite is zero. The T_0 temperature was obtained by a CALPHAD method [43]. The M_s temperature of the retained austenite phase in this material was – 22 °C, as mentioned in the Sect. 3.1.

For the temperature, T, the experimentally measured temperature data should be reflected as an input value. However, for a duration time of 0.1 s when the electric current was applied, it should not be calculated solely based on the measured temperature due to Joule heating. According to previous studies [20, 22, 28–30], it was commonly indicated that the athermal effect of electric current can obviously accelerate the microstructural changes through atomic diffusion, which is distinct from the thermal effect due to Joule heating. However, it is difficult to separate the athermal effect of electric current on MIMT kinetics from thermal effect during application of electric current in this study. Therefore, the calculation was performed only for the region where the electric current was eliminated.

Additionally, the functions of A and B in Eq. (3) were derived on the basis of the observation that the strain-induced nucleation occurs predominantly at shear-band intersections [44, 45]. They are expressed by the following formulas [40]:

$$A^i = -\frac{0.011\alpha\delta\gamma\left(f_{sb}\right)^{r-1}\left(1-f_{sb}\right)}{24\Delta S}\left(\Delta G + U^i\right), \tag{7}$$

$$B = -\frac{0.011[1+\delta\left(f_{sb}\right)^r]}{24\Delta S}, \tag{8}$$

where α is the shear-band formation rate, and δ and γ are the geometric constants. f_{sb} is the volume fraction of shear-bands. It is known that the parameter on the rate of shear-band formation, α, decreases with increasing temperature [44, 45]. These three material's parameters were adjusted to give the best agreement between the experimental data and calculated transformation kinetics data.

Thus, based on the extension of the classical Johnson–Mehl–Avrami–Kolmogrov (JMAK) theory for the simultaneous decomposition of austenite [46], the real volume fraction of ith martensitic variant at time, $t + dt$, can be obtained as:

$$f_{t+dt}^i = f_t^i + df^i, \tag{9}$$

$$df^i = \left(1 - \sum_{i=1}^{24} f_{t+dt}^i\right) df_{ex}^i. \tag{10}$$

Then, the total volume fraction of martensite in the retained austenite then becomes:

$$f = \sum_{i=1}^{24} f^i, \tag{11}$$

where f refers to the volume fraction of the martensite transformed from one parent austenite.

Finally, the total volume fraction of martensite, X_m, in the TRIP-aided steel specimen can be obtained as:

$$X_m = X_a^I f, \tag{12}$$

where X_a^I is the initial volume fraction of retained austenite in the TRIP-aided steel.

Table 1 Material's parameters in Eq. (7) for the investigated TRIP-aided steel

α	δ	r	T_0 (°C)	M_s (°C)
3244 $exp[-0.0208(T+273)]$	0.25	3.44	532	−22

Based on the above MIMT kinetic model, the MIMT kinetics for the given test conditions were calculated. The reliability of the experimental data for the retained austenite phase fraction was improved by comparing between the experimental data (symbols) and calculated data (lines) for the phase transformation kinetics, as shown in Figs. 5b and 6b. First, the material's parameters in Eq. (7) obtained from the result of non-puled tension at RT are listed in Table 1 and used in the calculation of MIMT kinetics for all test conditions.

As a result, as shown in Figs. 5b and 7b, the calculated and experimental data were in good agreement for all test conditions. This result shows that the MIMT kinetics of this material can be successfully described by the model. Moreover, it was obviously confirmed that the dominant suppression effect of the MIMT occurred in the multi-pulsed tension and a proper delay effect of the MIMT occurred in the 3-pulsed tension. However, one aspect needs to be noted. The athermal effect on MIMT during application of electric current was not considered in the present study. Thus, it could be thought that the athermal effect does not exist through the fact that the experimental value was well matched with the calculated value. However, since the current duration time of 0.1 s is quite short and the MIMT occurs during the cooling after applying the electric current, it appears as if there is no athermal effect. Thus, it should not be concluded that there is no athermal effect. A further quantitative analysis to distinguish the distinct electric current effect from thermal effect due to Joule heating in the MIMT kinetics for TRIP-aided steels is beyond the scope of the present study and will be reported in a separate study.

4 Conclusions

In the present study, the effect of electric current on the MIMT for TRIP-aided steel was investigated based on microstructural analysis and calculations. When a periodic pulsed electric current was applied to the specimen during plastic deformation, the elongation at fracture decreased compared to the non-pulsed tension at RT, although the flow stress substantially decreased. From the XRD measurement and calculation of MIMT kinetics, it was identified that the MIMT effect could not work properly in the multi-pulsed and non-pulsed tension at 100 °C, because the stability of the retained austenite phase increased due to a temperature rise.

A new pulsing pattern of electric current was designed to improve the formability of TRIP-aided steel. Three pulses of electric current were applied in the early stage of deformation immediately before the phase transformation of retained austenite phase begins to take place. As a result, a significant increase in elongation was observed compared to non-pulsed tension at RT. The increase in elongation in the 3-pulsed tension was due to two types of effect. One is the delay effect of the phase transformation, causing the MIMT effect to be exhibited in the latter stage of deformation. The other is an annealing effect during application of electric current, which is identified by comparing the FWHM values obtained from the XRD measurement.

Therefore, this study suggests that the effect of electric current on the mechanical behavior can be strongly affected by microstructural phenomena in the selected metal alloy under deformation. The EAM technique can efficiently improve the formability by designing the pulsing pattern of electric current in accordance with the material characteristic.

Acknowledgements This work was supported by the National Research Foundation of Korea (NRF) grants funded by the Ministry of Science and ICT (MSIT) (No. 2015R1A5A1037627 and No. 2018R1A2B6006856). H.N. Han and H.-J. Jeong were supported by POSCO research project. The Institute of Engineering Research at Seoul National University provided research facilities for this work.

References

1. Friedrich, H. E., Steinle, P., Kopp, G., & Scholl, R. (2010). Next decades 'Challenges for Terrestrial Vehicles' materials and manufacturing to reduce CO2 emissions. *Materials Science Forum, 3,* 638–642.
2. Jimenez-Melero, E., van Dijk, N. H., Zhao, L., Sietsma, J., Wright, J. P., & van der Zwaag, S. (2011). In situ synchrotron study on the interplay between martensite formation, texture evolution and load partitioning in low-alloyed TRIP steels. *Materials Science and Engineering A, 528,* 6407–6416.
3. Jacques, P., Ladriere, J., & Delannay, F. (2011). On the influence of interactions between phases on the mechanical stability of retained austenite in transformation-induced plasticity multiphase steels. *Metallurgical and Materials Transactions A: Physical Metallurgy and Materials Science, 32,* 2759–2768.
4. Tirumalasetty, G. K., Huis, M. A., van Kwakernaak, C., Sietsma, J., Sloof, W. G., & Zandbergen, H. W. (2012). Deformation-induced austenite grain rotation and transformation in TRIP-assisted steel. *Acta Materialia, 60,* 1311–1321.
5. Girault, E., Martens, A., Jacques, P., Houbaert, Y., Verlinden, B., & van Humbeeck, J. (2001). Comparison of the effects of silicon and aluminium on the tensile behaviour of multiphase TRIP-assisted steels. *Scripta Materialia, 44,* 885–892.
6. Jacques, P., Furnemont, Q., Mertens, A., & Delannay, F. (2001). On the sources of work hardening in multiphase steels assisted by transformation-induced plasticity. *Philosophical Magazine A, 81,* 1789–1812.
7. Han, H. N., & Lee, J. K. (2002). A constitutive model for transformation superplasticity under external stress during phase transformation of steels. *ISIJ International, 42,* 200–205.
8. Han, H. N., & Suh, D.-W. (2003). A model for transformation plasticity during bainite transformation of steel under external stress. *Acta Materialia, 51,* 4907–4917.
9. Zackay, V. F., Parker, E. R., Fahr, D., & Bush, R. (1967). The enhancement of ductility in high-strength steels. *Transactions of American Society for Metals*, *60,* 252–259.

10. Han, H. N., Oh, C.-S., Kim, G., & Kwon, O. (2009). Design method for TRIP-aided multiphase steel based on a microstructure-based modelling for transformation-induced plasticity and mechanically induced martensitic transformation. *Materials Science and Engineering A, 499,* 462–468.
11. Olson, G. B., & Cohen, M. (1982). Stress-assisted isothermal martensitic transformation: Application to TRIP steels. *Metallurgical and Materials Transactions A: Physical Metallurgy and Materials Science, 13,* 1907–1914.
12. Han, H. N., Lee, C. G., Suh, D.-W., & Kim, S.-J. (2008). A microstructure-based analysis for transformation induced plasticity and mechanically induced martensitic transformation. *Materials Science and Engineering A, 485,* 224–233.
13. Carlos, G.-M., & Francisca, G. C. (2005). The role of retained austenite on tensile properties of steels with bainitic microstructures. *Materials Transactions, 46,* 1839–1846.
14. Schubert, R. (2003). Warm forming—principles, applications, case study. Society of Manufacture Engineers, Technical papers, EM 87–129, pp. 1–15.
15. Troitskii, O. A. (1969). Electromechanical effect in metals. *Pis'ma v Zhurnal Èksperimental'noi i Teoreticheskoi Fiziki, 10,* 18–22.
16. Okazaki, K., Kagawa, M., & Conrad, H. (1978). A study of the electroplastic effect in metals. *Scripta Metallurgica, 12,* 1063–1068.
17. Conrad, H. (2000). Electroplasticity in metals and ceramics. *Materials Science and Engineering A, 287,* 276–287.
18. Ross, C., Roth, J.T. (2005). The effects of DC current on the tensile properties of metals. In *Proceedings of the ASME Materials Division Roth 100*, (pp. 363–372). New York: ASME.
19. Ross, C. D., Irvin, D. B., & Roth, J. T. (2007). Manufacturing aspects relating to the effects of direct current on the tensile properties of metals. *Journal of Engineering Materials and Technology, 129,* 342–347.
20. Kim, M.-J., Lee, K., Oh, K. H., Choi, I. S., Yu, H. H., Hong, S.-T., et al. (2014). Electric current-induced annealing during uniaxial tension of aluminum alloy. *Scripta Materialia, 75,* 58–61.
21. Tang, G., Zhang, J., Yan, Y., Zhou, H., & Fang, W. (2003). The engineering application of the electroplastic effect in the cold-drawing of stainless steel wire. *Journal of Materials Processing Technology, 137,* 96–99.
22. Kim, M.-S., Vinh, N. T., Yu, H.-H., Hong, S.-T., Lee, H.-W., Kim, M.-J., et al. (2014). Effect of electric current density on the mechanical property of ultra-high strength steels under quasi-static tensile loads. *International Journal of Precision Engineering and Manufacturing, 15,* 1207–1213.
23. Lu, W. J., & Qin, R. S. (2016). Stability of martensite with pulsed electric current in dual-phase steels. *Materials Science and Engineering A, 677,* 252–258.
24. Nguyen-Tran, H.-D., Oh, H.-S., Hong, S.-T., Han, H. N., Cao, J., Ahn, S.-H., et al. (2015). A review of electrically-assisted manufacturing. *International Journal of Precision Engineering and Manufacturing-Green Technology, 2,* 365–376.
25. Thien, N. T., Jeong, Y.-H., Hong, S.-T., Kim, M.-J., Han, H. N., & Lee, M.-G. (2016). Electrically assisted tensile behavior of complex phase ultra-high strength steel. *International Journal of Precision Engineering and Manufacturing-Green Technology, 3,* 325–333.
26. Magargee, J., Morestin, F., & Cao, J. (2013). Characterization of flow stress for commercially pure titanium subjected to electrically-assisted deformation. *Journal of Engineering Materials and Technology, 135,* 041003.
27. Magargee, J., Fan, R., & Cao, J. (2013). Analysis and observations of current density sensitivity and thermally activated mechanical behavior in electrically-assisted deformation. *Journal of Manufacturing Science and Engineering, 135,* 061022.
28. Kim, M.-J., Lee, M.-G., Hariharan, K., Hong, S.-T., Choi, I.-S., Kim, D. Y., et al. (2017). Electric current-assisted deformation behavior of Al-Mg-Si alloy under uniaxial tension. *International Journal of Plasticity, 94,* 148–170.
29. Jeong, H.-J., Kim, M.-J., Park, J.-W., Yim, C. D., Kim, J. J., Kwon, O. D., et al. (2017). Effect of pulsed electric current on dissolution of $Mg_{17}Al_{12}$ phases in as-extruded AZ91 magnesium alloy. *Materials Science and Engineering A, 684,* 668–676.
30. Park, J.-W., Jeong, H.-J., Jin, S.-W., Kim, M.-J., Lee, K., Kim, J. J., et al. (2017). Effect of electric current on recrystallization kinetics in interstitial free steel and AZ31 magnesium alloy. *Materials Characterization, 133,* 70–76.
31. Sprecher, A. F., Mannan, S. L., & Conrad, H. (1986). Overview no.49 on the mechanisms for the electroplastic effect in metals. *Acta Materialia, 37,* 1145–1162.
32. Boiko, Y. I., Geguzin, Y. E., & Klinchuk, Y. I. (1981). Drag of dislocations by an electron wind in metals. *Zhurnal Eksperimental'noi i Teoreticheskoi Fiziki, 81,* 2175–2179.
33. Molotskii, M. I., & Fleurov, V. (1995). Magnetic effects in electroplasticity of metals. *Physical Review B, 52,* 15829–15834.
34. Liu, X., Lan, S., & Ni, J. (2013). Experimental study of electroplastic effect on advanced high strength steels. *Materials Science and Engineering A, 582,* 211–218.
35. Lee, S.-J., Lee, S., & De Cooman, B. C. (2011). Mn partitioning during the intercritical annealing of ultrafine-grained 6% Mn transformation-induced plasticity steel. *Scripta Materialia, 64,* 649–652.
36. Mahieu, J., Maki, J., De cooman, B. C., & Claessens, S. (2002). Phase transformation and mechanical properties of Si-free CMnAl transformation-induced plasticity–aided steel. *Metallurgical and Materials Transactions A, 33,* 2573–2580.
37. Williamson, G. K., & Hall, W. H. (1953). X-ray line broadening from filed aluminium and wolfram. *Acta Metallurgica, 1,* 22–31.
38. Ungar, T., & Borbely, A. (1996). The effect of dislocation contrast on x-ray line broadening: A new approach to line profile analysis. *Applied Physics Letters, 69,* 3173–3175.
39. Ungar, T., Dragomir, I., Revesz, A., & Borbely, A. (1999). The contrast factors of dislocations in cubic crystals: the dislocation model of strain anisotropy in practice. *Journal of Applied Crystallography, 32,* 992–1002.
40. Han, H. N., Lee, C. G., Oh, C.-S., Lee, T.-H., & Kim, S.-J. (2004). A model for deformation behavior and mechanically induced martensitic transformation of metastable austenitic steel. *Acta Materialia, 52,* 5203–5214.
41. Furnemont, Q., Kempf, M., Jacques, P., Goken, M., & Delannay, F. (2002). On the measurement of the nanohardness of the constitutive phases of TRIP-assisted multiphase steels. *Materials Science and Engineering A, 328,* 26–32.
42. Jacchin, K., & Beyer, B. (2000). Thermodynamical calculation of martensite start temperatures in the system FeCrMnNiC. *Zeitschrift fuer Metallkunde, 91,* 106–113.
43. Sundman, B., Jansson, B., & Andersson, J. O. (1985). The thermo-calc databank system. *CALPHAD, 9,* 153–190.
44. Olson, G. B., & Cohen, M. (1975). Kinetics of strain induced martensitic nucleation. *Metallurgical Transactions, 6A,* 791–795.
45. Lecroisey, F., & Pineau, A. (1972). Martensitic transformations induced by plastic deformation in the Fe-Ni-Cr-C system. *Metallurgical Transactions, 3,* 387–396.
46. Jones, S. J., & Bhadeshia, K. H. D. H. (1997). Kinetics of the simultaneous decomposition of austenite into several transformation products. *Acta Metallurgica et Materialia, 45,* 2911–2920.

Hye-Jin Jeong Ph. D. candidate in Department of Materials Science & Engineering, Seoul National University. Her research interest is electroplasticity and microstructure for materials.

Nong Moon Hwang Professor in Department of Materials Science & Engineering, Seoul National University. His research interest is electronic materials and the theory of charged nanoparticles.

Ju-Won Park Ph. D. candidate in Department of Materials Science & Engineering, Seoul National University. His research interest is electro-treatment and microstructure for materials.

Sung-Tae Hong Professor in School of Mechanical Engineering, University of Ulsan. His research interest is process design and application of electrically assisted manufacturing.

Kyeong Jae Jeong Ph. D. candidate in Department of Materials Science & Engineering, Seoul National University. His research interest is material property prediction through multi-scale modeling.

Heung Nam Han Professor in Department of Materials Science & Engineering, Seoul National University. His research interest is mechanical behavior and microstructure for materials.